

A high order special relativistic hydrodynamic code with space-time adaptive mesh refinement

Olindo Zanotti^{a,*}, Michael Dumbser^a

^aLaboratory of Applied Mathematics, Department of Civil, Environmental and Mechanical Engineering, University of Trento, Via Mesiano 77, I-38123 Trento, Italy

Abstract

We present a high order one-step ADER-WENO finite volume scheme with space-time adaptive mesh refinement (AMR) for the solution of the special relativistic hydrodynamics equations. By adopting a local discontinuous Galerkin predictor method, a high order one-step time discretization is obtained, with no need for Runge-Kutta sub-steps. This turns out to be particularly advantageous in combination with space-time adaptive mesh refinement, which has been implemented following a “cell-by-cell” approach. As in existing second order AMR methods, also the present higher order AMR algorithm features time-accurate local time stepping (LTS), where grids on different spatial refinement levels are allowed to use different time steps.

We also compare two different Riemann solvers for the computation of the numerical fluxes at the cell interfaces. The new scheme has been validated over a sample of numerical test problems in one, two and three spatial dimensions, exploring its ability in resolving the propagation of relativistic hydrodynamical waves in different physical regimes. The astrophysical relevance of the new code for the study of the Richtmyer-Meshkov instability is briefly discussed in view of future applications.

Keywords: hydrodynamics, special relativity, high order ADER-WENO finite volume scheme, space-time Adaptive Mesh Refinement (AMR), time-accurate local time stepping (LTS)

1. Introduction

The numerical modeling of complex astrophysical flows that involve relativistic processes requires the development of more and more sophisticated codes. Relevant examples of relativistic phenomena whose understanding can greatly benefit from hydrodynamic and magnetohydrodynamic numerical simulations include extragalactic jets, gamma-ray-bursts, accretion onto compact objects, binary mergers of neutron stars (or black holes), relativistic heavy-ion collisions and so on.

Until few years ago, most of the applications in numerical relativistic hydrodynamic and magnetohydrodynamic used second-order accurate, typically TVD, numerical codes. The scientific progress that has been made possible by these implementations is rather significant and

*Corresponding author

Email addresses: olindo.zanotti@unitn.it (Olindo Zanotti), michael.dumbser@unitn.it (Michael Dumbser)

Preprint submitted to Elsevier

December 8, 2019

not always appreciated enough, see the living reviews by Martí and Müller (2003) and by Font (2008) plus references therein. However, the necessity of improving the accuracy of the computations, especially in the presence of complex phenomena such as instabilities or turbulence, combined with computational resources which are inevitably always limited, has motivated a strong research effort along two different directions. The first direction is represented by the development of high order schemes (better than second order in space and time), while the second direction consists in the implementation of efficient adaptive mesh refinement (AMR) algorithms. Taken separately, high order numerical schemes and AMR techniques have a long history, which is embarrassing to summarize in few words. The first high order special relativistic numerical scheme is due to Dolezal (1995), who, in the context of ultra-relativistic nuclear collision experiments, implemented a conservative finite difference scheme using ENO reconstruction in space and Runge–Kutta time integration, but without Riemann solvers. The first transposition of this approach to the astrophysical context is due to Del Zanna and Bucciantini (2002), who, in addition, used local Riemann problems to guarantee the upwind character of the scheme. Since then, several high order schemes have been proposed and applied to a variety of different astrophysical problems, both in the special and in the general relativistic regime [see Del Zanna et al. (2007), Tchekhovskoy et al. (2007), Bucciantini and Del Zanna (2011), Radice and Rezzolla (2011), Radice and Rezzolla (2012)]. Though different under many respects, a common feature of all these approaches is the use of a multi-step Runge–Kutta time integrator. A few years ago, Dumbser et al. (2008b) proposed an alternative idea for obtaining a high order integration in time, that avoids Runge–Kutta schemes altogether and originates from the ADER philosophy of Toro and Titarev (2002). According to this idea, which is followed also in this work, an arbitrary high order numerical scheme with just one step for the time update can be obtained, provided a high order time evolution is performed locally (namely within each cell), for the reconstructed polynomials. The first implementation of such ADER schemes in the context of ideal relativistic magnetohydrodynamics can be found in Dumbser et al. (2008a) and has later been successfully extended also to the non-ideal relativistic MHD equations in Dumbser and Zanotti (2009).

The implementation of AMR techniques has also a rich tradition in relativistic hydrodynamics and magnetohydrodynamics.¹ The first occurrence is documented in Winkler et al. (1984) followed by Dönmez (2004), Evans et al. (2005), van der Holst et al. (2008), Tao et al. (2008), Etienne et al. (2010), De Colle et al. (2012), Liebling et al. (2010), Lehner et al. (2012), East et al. (2012).

The combination of high order relativistic codes with AMR has a much more recent history. Relevant examples are given by the works of Mignone et al. (2012), who combined the AMR library CHOMBO, which originated from the original work of Berger and Olinger (1984), Berger (1986) and Berger and Colella (1989), with the versatile PLUTO code, using a Corner-Transport-Upwind scheme together with a third-order WENO reconstruction in space; Anderson et al. (2006), who solved the equations of general relativistic magnetohydrodynamics using a conservative finite difference scheme (with reconstruction of primitive variables plus Riemann solvers); Zhang and MacFadyen (2006), who implemented both a conservative finite difference scheme (with reconstruction of fluxes and no need for Riemann solvers) and a finite volume method, within the block-structured AMR package PARAMESH of MacNeice et al. (2000).

Contrary to the above mentioned approaches, all of them sharing a TVD Runge-Kutta for the time integration, in this paper we present an ADER-WENO finite volume scheme for solving the

¹We are not mentioning here the whole family of AMR implementations in vacuum space-times, namely without matter, which were initiated by Choptuik (1989).

special relativistic hydrodynamics equations, with adaptive mesh refinement. In Dumbser et al. (2013) we have proposed the first ADER-AMR finite volume numerical scheme for the Newtonian Euler equations and here we propose the relativistic extension of our new approach. The use of a one-step scheme in time allows the implementation of time-accurate local time stepping (LTS) in a very natural and straight forward manner and has already been successfully applied in the context of high order Discontinuous Galerkin schemes with LTS (see Dumbser et al. (2007); Taube et al. (2009); Lörcher et al. (2007); Gassner et al. (2008)).

The outline of this paper is the following. In Sect. 2 we briefly recall the conservative formulation of special relativistic hydrodynamics. Sect. 3 is devoted to the description of the numerical method, while Sect. 4 contains the results of the new scheme. Finally, Sect. 5 concludes our work, with a discussion about future astrophysical applications. In the following we will assume a signature $\{-, +, +, +\}$ for the space-time metric and we will use Greek letters μ, ν, λ, \dots (running from 0 to 3) for four-dimensional space-time tensor components, while Latin letters i, j, k, \dots (running from 1 to 3) will be employed for three-dimensional spatial tensor components. Moreover, we set the speed of light $c = 1$.

2. Special relativistic hydrodynamics

In the following we consider a perfect fluid in a Minkowski space-time with Cartesian coordinates, for which the metric is given by

$$ds^2 = g_{\mu\nu} dx^\mu dx^\nu = -dt^2 + dx^2 + dy^2 + dz^2. \quad (1)$$

The fluid is described by an energy momentum tensor $T^{\alpha\beta}$

$$T^{\alpha\beta} = \rho h u^\alpha u^\beta + p g^{\alpha\beta}, \quad (2)$$

where u^α is the four-velocity of the fluid, while ρ , $h = 1 + \epsilon + p/\rho$, ϵ and p are the rest-mass density, the specific enthalpy, the specific internal energy, and the thermal pressure, respectively. All these quantities are measured in the co-moving frame of the fluid. We assume the pressure is related to ρ and ϵ through the ideal-gas equation of state (EOS), i.e.

$$p = \rho\epsilon(\gamma - 1), \quad (3)$$

where γ is the (constant) adiabatic index of the gas. The equations of special relativistic hydrodynamics, which in covariant form are simply written as

$$\nabla_\alpha(\rho u^\alpha) = 0, \quad (4)$$

$$\nabla_\alpha T^{\alpha\beta} = 0, \quad (5)$$

were first transposed in conservative form by Martí et al. (1991) as

$$\partial_t \mathbf{u} + \partial_i \mathbf{f}^i = 0, \quad (6)$$

where the conservative variables and the correspondent fluxes in the i direction are given by

$$\mathbf{u} = \begin{bmatrix} D \\ S_j \\ E \end{bmatrix}, \quad \mathbf{f}^i = \begin{bmatrix} v^i D \\ W_j^i \\ S^i \end{bmatrix}. \quad (7)$$

The conservative variables (D, S_j, E) are related to the rest-mass density ρ , to the thermal pressure p and to the fluid velocity v_i by

$$D = \rho W, \quad (8)$$

$$S_i = \rho h W^2 v_i, \quad (9)$$

$$E = \rho h W^2 - p, \quad (10)$$

where $W = (1 - v^2)^{-1/2}$ is the Lorentz factor of the fluid with respect to the Eulerian observer at rest in the Cartesian coordinate system, and

$$W_{ij} \equiv \rho h W^2 v_i v_j + p \delta_{ij} \quad (11)$$

is the fully spatial projection of the energy-momentum tensor of the fluid [see also Del Zanna et al. (2007)]. As a hyperbolic system in conservative form, the equations (6) admit a well defined Jacobian matrix with a corresponding set of eigenvectors and eigenvalues. All these properties have been investigated deeply over the years, and we address the interested reader to Aloy et al. (1999); Martí and Müller (2003) and to Rezzolla and Zanotti (2013) for the mathematical aspects of such equations. We just comment here on the method adopted to invert the system (8)–(10), which is needed to recover the primitive variables (p, ρ, v_i) from the conservative variables (D, S_i, E) . As well known, in relativistic hydrodynamics such a conversion is not analytic, and a numerical root-finding approach is therefore needed. In our numerical code we have at disposal two alternative strategies, which perform equally well. The first one is due to Del Zanna et al. (2007), and it uses the property that, after introducing the variables $x = v^2$, $y = \rho h W^2$, the whole problem can be reduced to the solution of the system $F_1 = 0$ and $F_2 = 0$, where

$$F_1(x, y) = xy^2 - S^2, \quad (12)$$

$$F_2(x, y) = y - p - E, \quad (13)$$

where $S^2 = S^i S_i$. Moreover, since the pressure of the ideal gas EOS (3) can be written as

$$p = \frac{\gamma - 1}{\gamma} \left[y - \frac{S^2}{y} - D \sqrt{1 - S^2/y^2} \right], \quad (14)$$

the second equation of the system above, namely Eq. (13), further reduces to an equation in the single unknown y , which can be solved with any root-finding algorithm. The second strategy that we have implemented is instead very similar to that of Baiotti (2004) [see also Appendix D of Rezzolla and Zanotti (2013)] and it requires the numerical solution of the following equation

$$p - \bar{p}[\rho(\mathbf{u}, p), \epsilon(\mathbf{u}, p)] = 0, \quad (15)$$

where p is the unknown pressure and \bar{p} is the pressure as obtained through the equation of state (3) written in terms of the conserved variables \mathbf{u} and of p itself. In both the strategies just described, the standard Newton–Raphson method has been adopted, combined to a bisection step for those cases when the Newton–Raphson fails.

3. Numerical method

As written like in Eq. (6), the equations of special relativistic hydrodynamics can be solved through a modern version of the ADER approach, namely by combining a high order WENO

reconstruction in space with a local space-time Galerkin predictor strategy for the time update. In the following we provide a concise explanation of the overall procedure, addressing to the relevant literature for an extended discussion, and especially to Dumbser et al. (2008b), Dumbser and Zanotti (2009) and Dumbser et al. (2013).

3.1. The Finite volume approach

According to the standard finite volume approach, a one-step discretization of the system of hyperbolic conservation laws (6) is obtained by integration of the PDE over a space-time control volume $C_{ijkn} = [x_{i-\frac{1}{2}}; x_{i+\frac{1}{2}}] \times [y_{j-\frac{1}{2}}; y_{j+\frac{1}{2}}] \times [z_{k-\frac{1}{2}}; z_{k+\frac{1}{2}}] \times [t^n; t^{n+1}]$ as ²

$$\bar{\mathbf{u}}_{ijk}^{n+1} = \bar{\mathbf{u}}_{ijk}^n - \frac{\Delta t}{\Delta x_i} (\mathbf{f}_{i+\frac{1}{2},jk} - \mathbf{f}_{i-\frac{1}{2},jk}) - \frac{\Delta t}{\Delta y_j} (\mathbf{g}_{i,j+\frac{1}{2},k} - \mathbf{g}_{i,j-\frac{1}{2},k}) - \frac{\Delta t}{\Delta z_k} (\mathbf{h}_{i,j,k+\frac{1}{2}} - \mathbf{h}_{i,j,k-\frac{1}{2}}) \quad (16)$$

where

$$\bar{\mathbf{u}}_{ijk}^n = \frac{1}{\Delta x_i} \frac{1}{\Delta y_j} \frac{1}{\Delta z_k} \int_{x_{i-\frac{1}{2}}}^{x_{i+\frac{1}{2}}} \int_{y_{j-\frac{1}{2}}}^{y_{j+\frac{1}{2}}} \int_{z_{k-\frac{1}{2}}}^{z_{k+\frac{1}{2}}} \mathbf{u}(x, y, z, t^n) dz dy dx \quad (17)$$

is the spatial average of the solution in the element $I_{ijk} = [x_{i-\frac{1}{2}}; x_{i+\frac{1}{2}}] \times [y_{j-\frac{1}{2}}; y_{j+\frac{1}{2}}] \times [z_{k-\frac{1}{2}}; z_{k+\frac{1}{2}}]$ at time t^n , while

$$\mathbf{f}_{i+\frac{1}{2},jk} = \frac{1}{\Delta t} \frac{1}{\Delta y_j} \frac{1}{\Delta z_k} \int_{t^n}^{t^{n+1}} \int_{y_{j-\frac{1}{2}}}^{y_{j+\frac{1}{2}}} \int_{z_{k-\frac{1}{2}}}^{z_{k+\frac{1}{2}}} \tilde{\mathbf{f}}_{\text{RP}}(x_{i+\frac{1}{2}}, y, z, t) dz dy dt, \quad (18)$$

$$\mathbf{g}_{i,j+\frac{1}{2},k} = \frac{1}{\Delta t} \frac{1}{\Delta x_i} \frac{1}{\Delta z_k} \int_{t^n}^{t^{n+1}} \int_{x_{i-\frac{1}{2}}}^{x_{i+\frac{1}{2}}} \int_{z_{k-\frac{1}{2}}}^{z_{k+\frac{1}{2}}} \tilde{\mathbf{g}}_{\text{RP}}(x, y_{j+\frac{1}{2}}, z, t) dz dx dt, \quad (19)$$

$$\mathbf{h}_{i,j,k+\frac{1}{2}} = \frac{1}{\Delta t} \frac{1}{\Delta x_i} \frac{1}{\Delta y_j} \int_{t^n}^{t^{n+1}} \int_{x_{i-\frac{1}{2}}}^{x_{i+\frac{1}{2}}} \int_{y_{j-\frac{1}{2}}}^{y_{j+\frac{1}{2}}} \tilde{\mathbf{h}}_{\text{RP}}(x, y, z_{k+\frac{1}{2}}, t) dy dx dt \quad (20)$$

are the space-time averaged numerical fluxes, with $\tilde{\mathbf{f}}_{\text{RP}}(x_{i+\frac{1}{2}}, y, z, t)$ being a numerical flux function, which is obtained by solving the Riemann problem at an element interface either exactly or approximately at a generic time t . Equation (16) has been derived directly from the conservation equations and is an exact integral relation. In order to be used as a high order numerical one-step scheme in space and time, a number of actions must be taken. The first one consists of a high order reconstruction of the solution within each control volume I_{ijk} , starting from the known cell averages $\bar{\mathbf{u}}_{ijk}^n$, which are the only quantities that are directly evolved in time via Eq. (16). Such a reconstruction is performed through a high order weighted essentially non-oscillatory (WENO) interpolation, and provides a polynomial representation of the solution, as we will discuss below.

²To keep the notation simpler, in the following we avoid the Einstein summation convention for the flux components, by writing explicitly $\mathbf{f} = \mathbf{f}^x, \mathbf{g} = \mathbf{f}^y, \mathbf{h} = \mathbf{f}^z$.

The second action consists of computing, locally for each space-time cell C_{ijkn} , the time evolution of the reconstructed polynomial, which in the following we denote as $\mathbf{q}_h(x, y, z, t)$. This, in turns, allows to compute the solution of the Riemann problem at the cell interfaces as

$$\tilde{\mathbf{f}}_{\text{RP}} = \tilde{\mathbf{f}}(\mathbf{q}_h^-(x_{i+\frac{1}{2}}, y, z, t), \mathbf{q}_h^+(x_{i+\frac{1}{2}}, y, z, t)), \quad (21)$$

where \mathbf{q}_h^- and \mathbf{q}_h^+ are the left and right boundary extrapolated states at the interface, respectively. The form of the function $\tilde{\mathbf{f}}$ depends of course on the specific choice of the Riemann solver adopted. Although an exact Riemann solver for special relativistic hydrodynamics has been known for years (Martí and Müller, 1994; Rezzolla and Zanotti, 2001), faster approximate Riemann solvers are typically preferred. In our calculations we have adopted two of them. The first one is the popular HLL Riemann solver by Harten et al. (1983), which does not rely on the characteristic structure of the equations and only needs the knowledge of the fastest and of the slowest eigenvalue. The second one is the Osher-type Riemann solver in the version proposed by Dumbser and Toro (2011) and it is based on the knowledge of the full spectral decomposition of the equations. Unlike the Roe Riemann solver, however, it is entropy-satisfying and thus does not produce unphysical rarefaction shocks.

3.2. A dimension-by-dimension WENO reconstruction

The WENO reconstruction that we have implemented is genuinely multi-dimensional, but, from an operational point of view, it works in a dimension-by-dimension fashion. In practice, focusing on the x direction for convenience, we first introduce a reference coordinate

$$x = x_{i-\frac{1}{2}} + \xi \Delta x_i, \quad (22)$$

where $\xi \in [0; 1]$. After that, we choose the degree M of the polynomial approximating the solution, and an orthogonal basis of polynomials (Solin, 2006), all of degree M , rescaled on the same unit interval $[0; 1]$. The basis is formed by the $M + 1$ Lagrange interpolation polynomials, $\{\psi_l(\lambda)\}_{l=1}^{M+1}$, passing through the $M + 1$ Gauss-Legendre quadrature nodes $\{\lambda_k\}_{k=1}^{M+1}$ and with the standard property that

$$\psi_l(\lambda_k) = \delta_{lk} \quad l, k = 1, 2, \dots, M + 1. \quad (23)$$

Having done that, a (small) number of one-dimensional reconstruction stencils is adopted, each of them given by the union of $M + 1$ adjacent cells, i.e.

$$\mathcal{S}_{ijk}^{s,x} = \bigcup_{e=i-L}^{i+R} I_{ejk}, \quad (24)$$

where $L = L(M, s)$ and $R = R(M, s)$ are the spatial extension of the stencil to the left and to the right. In practice, we have adopted the pragmatic approach for which odd order schemes (even polynomials of degree M) always use three stencils ($N_s = 3$), while even order schemes (odd polynomials of degree M) always adopt four stencils ($N_s = 4$) [see Dumbser et al. (2013) for more details].

With all this machinery at hands, we use the polynomial basis functions to reconstruct the solution at time t^n as³

$$\mathbf{w}_h^{s,x}(x, t^n) = \sum_{p=0}^M \psi_p(\xi) \hat{\mathbf{w}}_{ijk,p}^{n,s} := \psi_p(\xi) \hat{\mathbf{w}}_{ijk,p}^{n,s}. \quad (25)$$

³Note that here, and in the following, the Einstein summation convention is used over the repeated index p , even if such an index does not denote the covariant and contravariant components of a tensor.

As usual for finite volume methods, the reconstructed polynomial must preserve the cell-average of the solution over each element I_{ijk} , namely

$$\frac{1}{\Delta x_e} \int_{x_{e-\frac{1}{2}}}^{x_{e+\frac{1}{2}}} \psi_p(\xi(x)) \hat{\mathbf{w}}_{ijk,p}^{n,s} dx = \bar{\mathbf{u}}_{e,jk}^n, \quad \forall I_{e,jk} \in \mathcal{S}_{ijk}^{s,x}, \quad (26)$$

which provide a system of linear equations for the unknown coefficients $\hat{\mathbf{w}}_{ijk,p}^{n,s}$. This operation is repeated for each stencil relative to the element I_{ijk} . After that, we can construct a data-dependent nonlinear combination of the polynomials obtained from each stencil, i.e.

$$\mathbf{w}_h^x(x, t^n) = \psi_p(\xi) \hat{\mathbf{w}}_{ijk,p}^n, \quad \text{with} \quad \hat{\mathbf{w}}_{ijk,p}^n = \sum_{s=1}^{N_s} \omega_s \hat{\mathbf{w}}_{ijk,p}^{n,s}. \quad (27)$$

We refer to Dumbser et al. (2008b) for a detailed discussion about the choice of the nonlinear weights ω_s to be used in Eq. (27). We emphasize that the resulting reconstruction polynomial $\mathbf{w}_h^x(x, t^n)$ is still an average in the y and z directions. Hence, the procedure explained so far is repeated along the two missing directions y and z . We stress that the net effect of this approach is to provide a genuine multidimensional reconstruction, although in such a way that each direction is treated separately. Details about this strategy can be found in Dumbser et al. (2013).

3.3. The local space-time DG approach

The high order computation of the numerical fluxes (18)–(20), which contain a time integration from t^n to t^{n+1} , requires the numerical flux (Riemann solver) $\tilde{\mathbf{f}}_{\text{RP}}$ to be computed with high accuracy at any time in the interval $t \in [t^n, t^{n+1}]$. To this extent, we need an operation, to be performed locally for each cell, which uses as input the high order polynomial \mathbf{w}_h obtained from the WENO reconstruction, and gives as output its evolution in time, namely

$$\mathbf{w}_h(x, y, z, t^n) \longrightarrow \mathbf{q}_h(x, y, z, t). \quad (28)$$

Unlike the original ADER approach, where this operation was obtained through the so called Cauchy-Kovalewski procedure (Toro and Titarev, 2005; Dumbser et al., 2007), in the modern version of ADER the transformation represented by (28) is obtained through an element–local space–time Discontinuous Galerkin predictor that is based on the *weak* integral form of Eq. (6). This idea was first proposed by Dumbser et al. (2008b) and additional details about it can be found in Dumbser et al. (2013). We just note that the sought polynomial $\mathbf{q}_h(x, y, z, t)$ is expanded as

$$\mathbf{q}_h = \mathbf{q}_h(\xi, \tau) = \theta_p(\xi, \tau) \hat{\mathbf{q}}_p, \quad (29)$$

where the polynomial basis functions θ_p are given by a tensor–product of the basis functions ψ_l already used for the WENO reconstruction, namely

$$\theta_p(\xi, \tau) = \psi_p(\xi) \psi_q(\eta) \psi_r(\zeta) \psi_s(\tau). \quad (30)$$

The computation of the unknown degrees of freedom $\hat{\mathbf{q}}_p$ requires the solution of an algebraic system of equations, obtained through standard iterative procedures. The proposed approach has been shown to cope successfully even with stiff source terms (Dumbser and Zanotti, 2009; Zanotti and Dumbser, 2011). However, there is no such a necessity in the case of special relativistic hydrodynamics, whose source terms vanish in Cartesian coordinates.

3.4. Adaptive mesh refinement

AMR algorithms can be roughly divided in two main categories. In the first category, nested arrays of logically rectangular grid patches are used, according to the original Berger-Colella-Oliger approach (Berger and Oliger, 1984; Berger and Colella, 1989). In the second category, a 'cell-by-cell' refinement is instead adopted, and the resulting cells are managed as elements of a tree-data structure. It is in this version that AMR techniques were first applied to astrophysics, for performing N-body cosmological simulations (Khokhlov et al., 1997), and this is also the strategy that we have implemented. We refer to Dumbser et al. (2013) for a detailed description of our AMR algorithm, which was extensively validated for the classical Euler and magneto-hydrodynamics equations. We just recall here that, as in any other AMR algorithm, there are a number of free parameters, namely

- The maximum level of refinement ℓ_{\max} , typically 2 or 3 in our tests.
- The refinement factor τ , governing the number of sub-cells that are generated according to

$$\Delta x_\ell = \tau \Delta x_{\ell+1} \quad \Delta y_\ell = \tau \Delta y_{\ell+1} \quad \Delta z_\ell = \tau \Delta z_{\ell+1}, \quad (31)$$

where Δx_ℓ is size of the cell, at ℓ refinement level, along the x -direction, and similarly for the other directions.

- The choice of the refinement criterion, which in our approach is simply feature-based and uses the calculation of a second derivative, see Löhner (1987). In practice, a cell C_m is marked for refinement if $\chi_m > \chi_{\text{ref}}$, while it is marked for recoarsening if $\chi_m < \chi_{\text{rec}}$, where

$$\chi_m = \sqrt{\frac{\sum_{k,l} (\partial^2 \Phi / \partial x_k \partial x_l)^2}{\sum_{k,l} [(|\partial \Phi / \partial x_k|_{i+1} + |\partial \Phi / \partial x_k|_i) / \Delta x_l + \varepsilon |(\partial^2 / \partial x_k \partial x_l)| |\Phi|]}}, \quad (32)$$

The summation $\sum_{k,l}$ is taken over the number of space dimension of the problem in order to include the cross term derivatives. The function $\Phi = \Phi(\mathbf{u})$ can be any suitable indicator function of the conservative variables \mathbf{u} . We have observed that the threshold values χ_{ref} and χ_{rec} can be slightly model dependent. In most of our tests we have chosen χ_{ref} in the range $\sim [0.2, 0.25]$ and χ_{rec} in the range $\sim [0.05, 0.15]$. Finally, the parameter ε acts as a filter preventing refinement in regions of small ripples and is given the value $\varepsilon = 0.01$. In alternative, we refer the reader to the use of error based adaptation as investigated by Baeza et al. (2012) in the context of the high order WENO AMR schemes first proposed by Baeza and Mulet (2006).

4. Numerical tests

4.1. One-dimensional isentropic flow

The first test that we have considered, already studied by Zhang and MacFadyen (2006) and Radice and Rezzolla (2012), describes a one-dimensional simple wave (Anile, 1990), namely a smooth solution for which two, out of the three, Riemann invariants associated to the acoustic eigenvalues are constant. Such Riemann invariants are the specific entropy s and one of the two quantities

$$J_\pm = \frac{1}{2} \ln \left(\frac{1+v}{1-v} \right) \pm \frac{1}{\sqrt{\gamma-1}} \ln \left(\frac{\sqrt{\gamma-1} + c_s}{\sqrt{\gamma-1} - c_s} \right), \quad (33)$$

Table 1: Numerical convergence results for the isentropic one-dimensional test using the third, the fourth and the fifth order version of the one-step ADER-WENO finite volume scheme. The norms refer to the rest-mass density at the final time $t = 1$. Only uniform grids (no AMR) have been used.

N_G	$L_2(\rho)$	$O(L_2)$
$O3$		
128	2.32645002570E+00	
256	2.32649582331E+00	
512	2.32650702640E+00	2.03
1024	2.32650877354E+00	2.68
2048	2.32650899401E+00	2.99
4096	2.32650902270E+00	2.94
$O4$		
128	2.32647589689E+00	
256	2.32650584299E+00	
512	2.32650892215E+00	3.28
1024	2.32650902130E+00	4.96
2048	2.32650902669E+00	4.20
4096	2.32650902682E+00	5.32
$O5$		
128	2.32649009926E+00	
256	2.32650682213E+00	
512	2.32650894845E+00	2.98
1024	2.32650902359E+00	4.82
2048	2.32650902673E+00	4.58
4096	2.32650902682E+00	5.12

where the sound speed c_s is given by

$$c_s^2 = \frac{\gamma p}{h\rho} = \frac{\gamma(\gamma - 1)p}{\gamma p + (\gamma - 1)\rho}. \quad (34)$$

In our calculations, we have chosen J_- as constant, hence describing an isentropic right-propagating simple wave (Anile et al., 1983). Consistently with these assumptions, the fluid obeys a poly-tropic equation of state of the type

$$p = K\rho^\gamma. \quad (35)$$

The initial profile of the rest-mass density is chosen as in Radice and Rezzolla (2012), i.e.

$$\rho(x, 0) = \begin{cases} 1 + \exp[-1/(1 - x^2/L^2)] & \text{for } |x| < L, \\ 1 & \text{for } |x| > L, \end{cases} \quad (36)$$

where L determines the width of the profile. Since $\rho(x, 0) = 1$ and $v(x, 0) = 0$ for $|x| > L$, Eq. (33) can be used to compute the value of J_- and, consequently, the profile of the initial velocity in the range $-L < x < L$. As the wave propagates towards the right, steepening occurs until a shock wave forms. In our calculations we have solved the problem over the computational domain

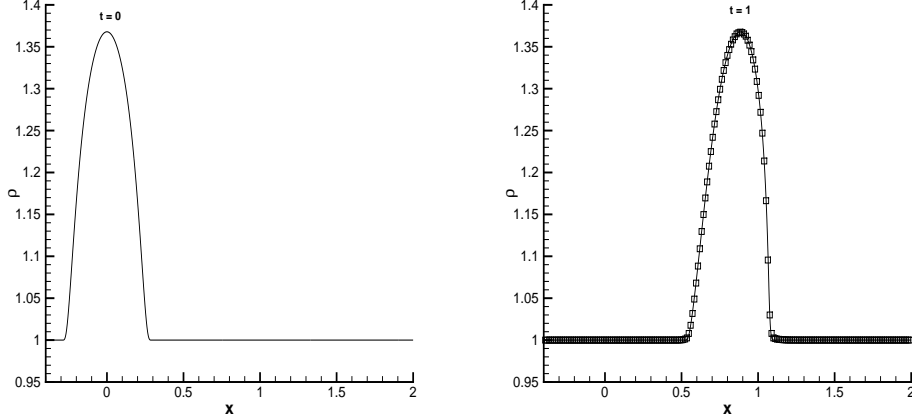


Figure 1: Isentropic one-dimensional flow. Left panel: initial profile of the rest-mass density. Right panel: solution at time $t = 1.0$ obtained with the fifth order ADER-WENO scheme.

$-0.4 < x < 2.0$ up to time $t = 1.0$ (before the shock formation) and we have used $K = 100$, $\gamma = 5/3$, $L = 0.3$. To validate our procedure, we have first considered a sequence of uniform grids and computed an estimate of the numerical order of convergence according to

$$O \sim \log_2 \frac{\|L_{\Delta x}\| - \|L_{\Delta x/2}\|}{\|L_{\Delta x/2}\| - \|L_{\Delta x/4}\|}, \quad (37)$$

where $\|L_{\Delta x}\|$ is the 2-norm of a representative quantity, typically the rest-mass density, over a mesh with grid-size Δx . The estimates computed in this way using the Osher-type Riemann solver are reported in Tab. 1, which essentially confirms the nominal order of convergence.

After that, we have evolved these initial conditions with a truly adaptive grid, using a fifth order ADER-WENO scheme and with the relevant AMR parameters given by $\ell_{\max} = 2$, $\tau = 3$ and CFL = 0.8. Fig.1 shows the results of this calculation, where the left panel reports the initial condition, while the right panel depicts the solution at the final time, compared to a reference solution which has been obtained using a highly refined mesh with a standard second-order TVD method.

4.2. One-dimensional Riemann problems

To further validate the new scheme, we have considered a set of relativistic shock tubes, with initial conditions reported in Table 2. In all cases the numerical solution has been computed both with the HLL and with the Osher-type Riemann solver, and has been compared to the exact solution computed according to the procedure outlined in Rezzolla and Zanotti (2001).

Problem 1, considered also by Mignone and Bodo (2005), has initial conditions producing a wave-pattern that consists of two rarefaction waves (henceforth, a $2\mathcal{R}$ wave-pattern), propagating to the left and to the right, and the usual contact discontinuity between them. A fourth order WENO scheme with $\ell_{\max} = 2$, $\tau = 3$ and CFL = 0.6 has been used. The results of this test are

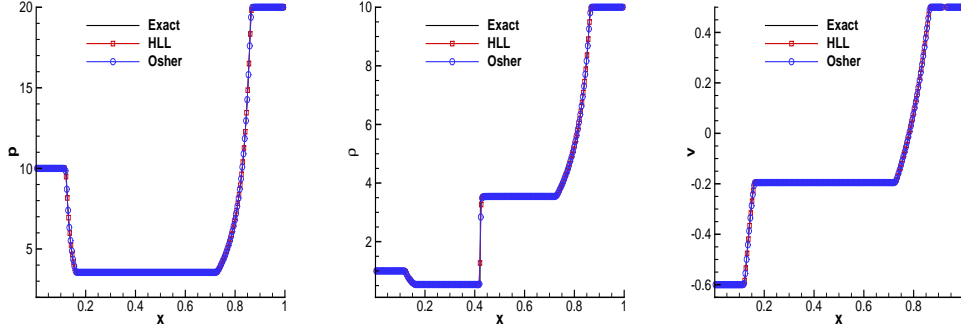


Figure 2: Solution of Problem 1 with the fourth order ADER-WENO scheme at time $t = 0.4$.

shown in Fig. 2, with HLL and Osher fluxes reproducing the exact solution with essentially the same accuracy.

Problem 2, considered also by Radice and Rezzolla (2012), has initial conditions producing a wave-pattern that consists of a rarefaction wave, propagating to the left, a contact discontinuity and a shock wave propagating to the right (henceforth, a \mathcal{RS} wave-pattern). The shock wave is characterized by a strong density contrast. A fourth order WENO scheme with $\ell_{\max} = 2$, $\tau = 3$ and $\text{CFL} = 0.6$ has been used. The results of this test are shown in Fig. 3. We note that in this case the Osher flux gives a slightly better representation of the blast wave, as can be seen from the inset in the central panel.

Problem 3, considered also by Zhang and MacFadyen (2006), has initial conditions producing a wave-pattern that consists of two shock waves, propagating to the left and to the right, plus again the contact discontinuity between them (henceforth, a $2\mathcal{S}$ wave-pattern). A fourth order WENO scheme with $\ell_{\max} = 2$, $\tau = 3$ and $\text{CFL} = 0.6$ has been used. The results of this test are shown in Fig. 4. We note that some oscillations appear in the post-shock region of the right-propagating shock, which are particularly visible in the rest mass density and in the pressure. Such oscillations are stronger for the Osher flux than for the more dissipative HLL flux.

4.3. One-dimensional Riemann problems with tangential velocities

In spite of the obvious additional complications introduced by special relativity, the one-dimensional Riemann problem without tangential velocities does not introduce qualitative dif-

Table 2: Initial left (L) and right (R) states of the relativistic shock tube problems. The last two columns report the adiabatic index and the final time t_f of the simulation.

Problem	ρ_L	v_L	p_L	ρ_R	v_R	p_R	γ	t_f
1	1	-0.6	10	10	0.5	20	5/3	0.4
2	10^{-3}	0	1	10^{-3}	0	10^{-5}	5/3	0.4
3	1	0.9	1	1	0	10	4/3	0.4

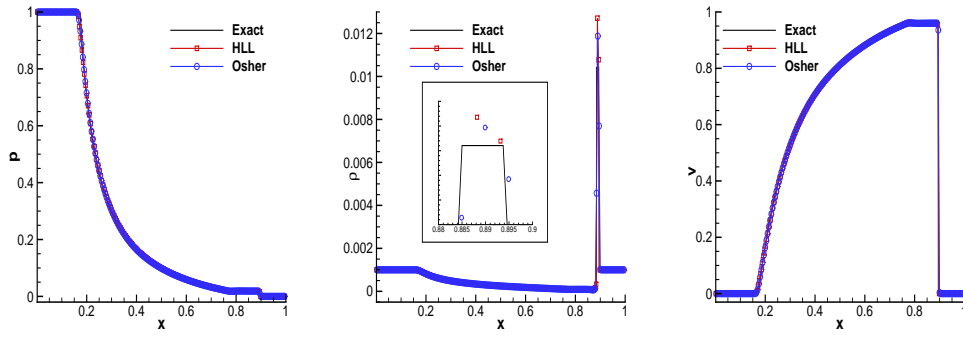


Figure 3: Solution of Problem 2 with the fourth order ADER-WENO scheme at time $t = 0.4$.

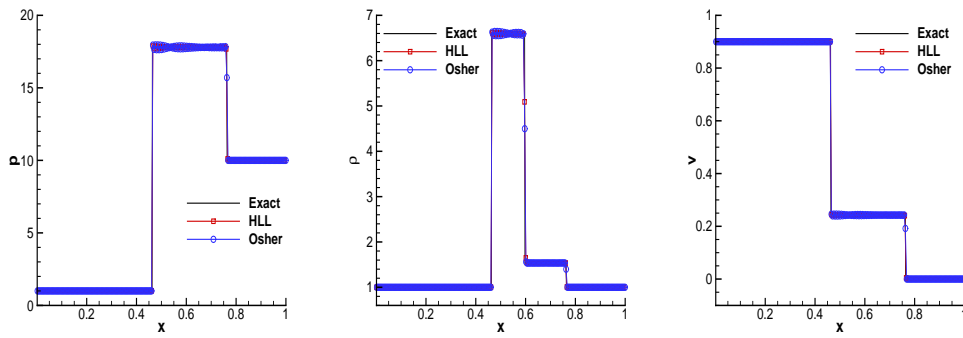


Figure 4: Solution of Problem 3 with the fourth order ADER-WENO scheme at time $t = 0.4$.

ferences with respect to its Newtonian analog. The situation changes drastically when tangential velocities are present.⁴ As shown by Rezzolla and Zanotti (2002), the coupling of the velocity components through the Lorentz factor is responsible of a new effect which is not present in Newtonian hydrodynamics. Namely, given a Riemann problem with initial conditions producing a \mathcal{RS} wave pattern and a non zero relative velocity along the normal direction, it is always possible to transform it into a $2\mathcal{S}$ wave-pattern by increasing the value of the initial tangential velocity in the state of initial *lower* pressure, while keeping the rest of the variables unmodified. Similarly, given a Riemann problem with initial conditions producing a \mathcal{RS} wave pattern and a non zero relative velocity along the normal direction, it is always possible to transform it into a $2\mathcal{R}$ wave-pattern by increasing the value of the initial tangential velocity in the state of initial *higher* pressure. Besides being at the heart of a possible acceleration mechanism in relativistic jets (Aloy and Rezzolla, 2006), this physical effect is also interesting from a numerical point of view, since it can be used to test the ability of a relativistic code in treating dynamical systems with fully coupled velocities.

We have simulated one such relevant example that has the following initial conditions

$$(\rho, v_x, v_t, p) = \begin{cases} (1.0, 0.8, 0.0, 1000.0) & \text{for } x < 0.5, \\ (1.0, 0.0, 0.999, 0.01) & \text{for } x > 0.5, \end{cases} \quad (38)$$

and adiabatic index $\gamma = 5/3$. In the absence of tangential velocities, namely when $v_t = 0$ on both initial states, the solution to this Riemann problem would consist of a \mathcal{RS} wave-pattern. However, due to the high value of v_t on the right state, the wave-pattern changes to a $2\mathcal{S}$ one. The solution is reported in Fig. 5, which also shows the reference solution computed according to Rezzolla et al. (2003). A third order WENO scheme with $\ell_{\max} = 2$, $\tau = 3$ and CFL = 0.6 has been used, proving the ability of the code in treating configurations with highly coupled velocity components. We note that for this test the HLL and the Osher-type Riemann solver provides essentially the same accuracy and only the data obtained with HLL have been plotted in the figure.

4.4. Two-dimensional Riemann problem

We solve the two-dimensional Riemann problem originally proposed by Del Zanna and Bucciantini (2002), and later reproduced by Lucas-Serrano et al. (2004), Mignone and Bodo (2005), Zhang and MacFadyen (2006). The initial conditions are prescribed over the square $[-1, 1] \times [-1, 1]$ and are given by

$$(\rho, v_x, v_y, p) = \begin{cases} (0.1, 0.99, 0, 1) & \text{for } x < 0, y > 0, \\ (0.1, 0, 0, 0.01) & \text{for } x > 0, y > 0, \\ (0.5, 0, 0, 1) & \text{for } x < 0, y < 0, \\ (0.1, 0, 0.99, 1) & \text{for } x > 0, y < 0, \end{cases} \quad (39)$$

with adiabatic index $\gamma = 5/3$. As the system evolves in time, two curved shock fronts propagate in the upper-right quadrant, while a jet-like structure emerges along the main diagonal. We have solved this problem with a third order WENO scheme applied to the characteristic variables and

⁴ A velocity component is tangential if it belongs to the plane normal to the discontinuity front.

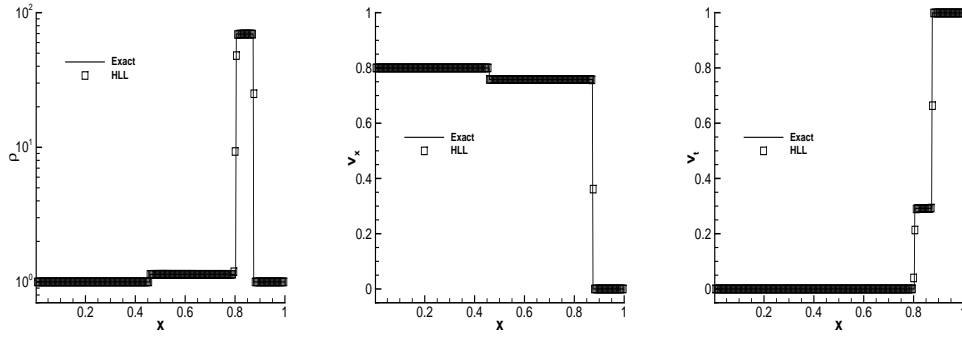


Figure 5: Solution of the Riemann problem with a non-zero tangential velocity at time $t = 0.4$. A third order ADER-WENO scheme has been used.

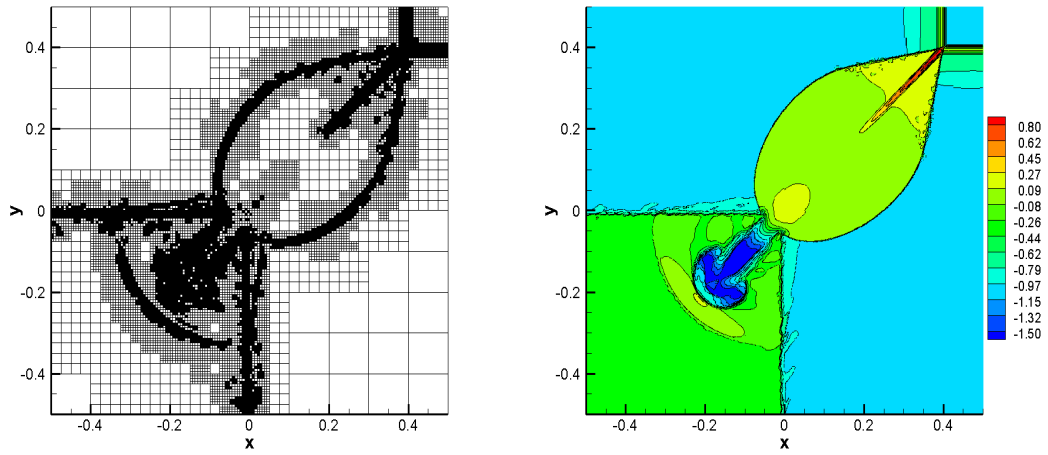


Figure 6: Solution of the 2D Riemann Problem obtained with a third order ADER-WENO scheme at time $t = 0.4$. Left panel: snapshot of the AMR grid. Right panel: logarithm of the rest mass density.

using the HLL Riemann solver. The grid is initially uniform with 20×20 cells. Three levels of refinement have been adopted, with $\tau = 4$ and $\text{CFL} = 0.4$. The results of our computations are reported in Fig.6, which shows the contour-plot of the rest mass density (right panel) and the corresponding AMR grid (left panel) at the final time $t = 0.4$. We stress that, in a limited number of troubled cells close to the corner $(0, 0)$, the accuracy of the solution has been intentionally reduced to first-order following a MOOD-type approach [see Clain et al. (2011)], to avoid the appearance of strong oscillations. In spite of this, the solution is very well reproduced by our numerical scheme.

4.5. Relativistic Kelvin–Helmholtz instability

The Kelvin–Helmholtz (KH) instability is a classical instability of fluid dynamics and in the astrophysical context is currently invoked to explain the observed phenomenology of extended radio-jets [see Martí and Müller (2003) and references therein]. In this section we present a simple test performed in two dimensions, where the linear growth phase of the KH instability is reproduced. Following the works of Mignone et al. (2009), Beckwith and Stone (2011) and Radice and Rezzolla (2012), we choose the initial conditions as

$$v^x = \begin{cases} v_s \tanh [(y - 0.5)/a] & y > 0, \\ -v_s \tanh [(y + 0.5)/a] & y \leq 0, \end{cases} \quad (40)$$

where $v_s = 0.5$ is the velocity of the shear layer and $a = 0.01$ is its characteristic size. In order to trigger the instability, a perturbation in the transverse velocity is introduced as

$$v^y = \begin{cases} \eta_0 v_s \sin(2\pi x) \exp[-(y - 0.5)^2/\sigma] & y > 0, \\ -\eta_0 v_s \sin(2\pi x) \exp[-(y + 0.5)^2/\sigma] & y \leq 0, \end{cases} \quad (41)$$

where $\eta_0 = 0.1$ is the amplitude of the perturbation, while $\sigma = 0.1$ is its length scale. Finally, the rest-mass density is chosen as

$$\rho = \begin{cases} \rho_0 + \rho_1 \tanh [(y - 0.5)/a] & y > 0, \\ \rho_0 - \rho_1 \tanh [(y + 0.5)/a] & y \leq 0, \end{cases} \quad (42)$$

with $\rho_0 = 0.505$ and $\rho_1 = 0.495$. The adiabatic index is $\gamma = 4/3$ and the pressure is $p = 1$ everywhere.

We have solved this problem on a rectangular domain $[-0.5, 0.5] \times [-1, 1]$, starting from an initial uniform grid with resolution 80×160 and adopting periodic boundary conditions both in x and in y directions. A third order ADER-WENO has been chosen and AMR is activated with relevant parameters $\ell_{\max} = 2$ and $\text{CFL}=0.8$. The results of our computations are reported in Fig. 7 and in Fig. 8, which refer to a refinement factor $\tau = 3$ and $\tau = 4$, respectively. In each figure the left panels display the AMR grid at time $t = 3$ while the right panels display the corresponding distribution of the rest–mass density. Finally, the top and the bottom panels refer to the HLL Riemann solver and to the Osher-type Riemann solver, respectively. In all cases we have performed reconstruction on the characteristic variables. At least two comments can be made about these results. First, the more diffusive HLL Riemann solver does not allow for the development of secondary small-scale instabilities along the shear layer (compare the top and the

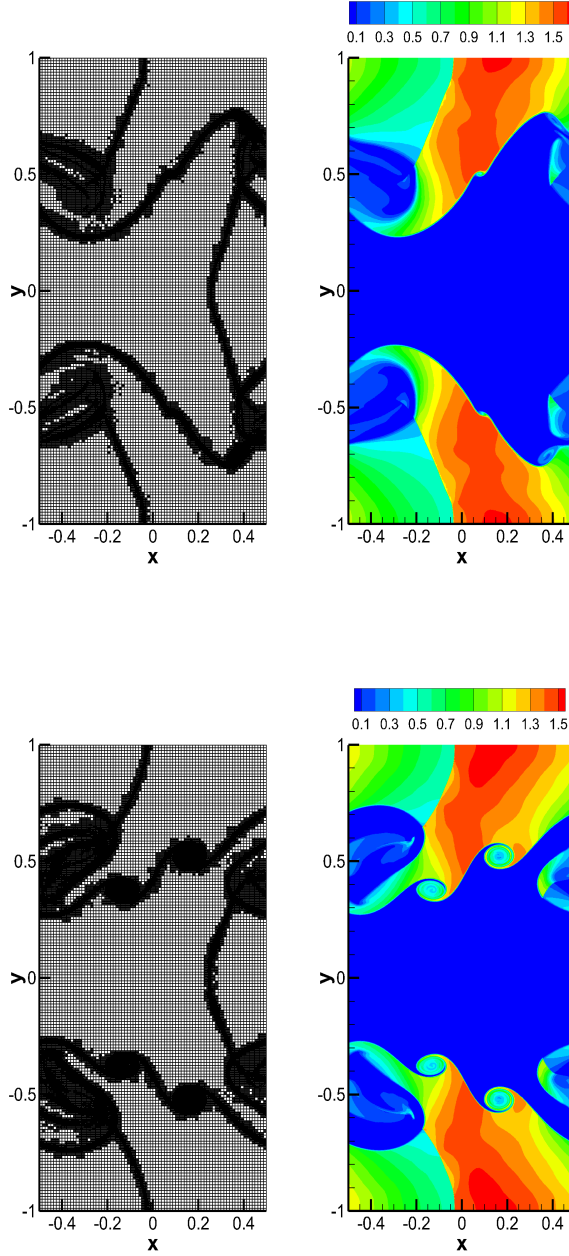


Figure 7: Two-dimensional Kelvin-Helmholtz instability at $t = 3.0$ with **refinement factor** $\tau = 3$. Left panels: the AMR grid. Right panels: the distribution of the rest-mass density. Top panels: results obtained with the HLL Riemann solver. Bottom panels: results obtained with the Osher Riemann solver. In both cases a third order ADER-WENO with CFL=0.8 has been adopted.

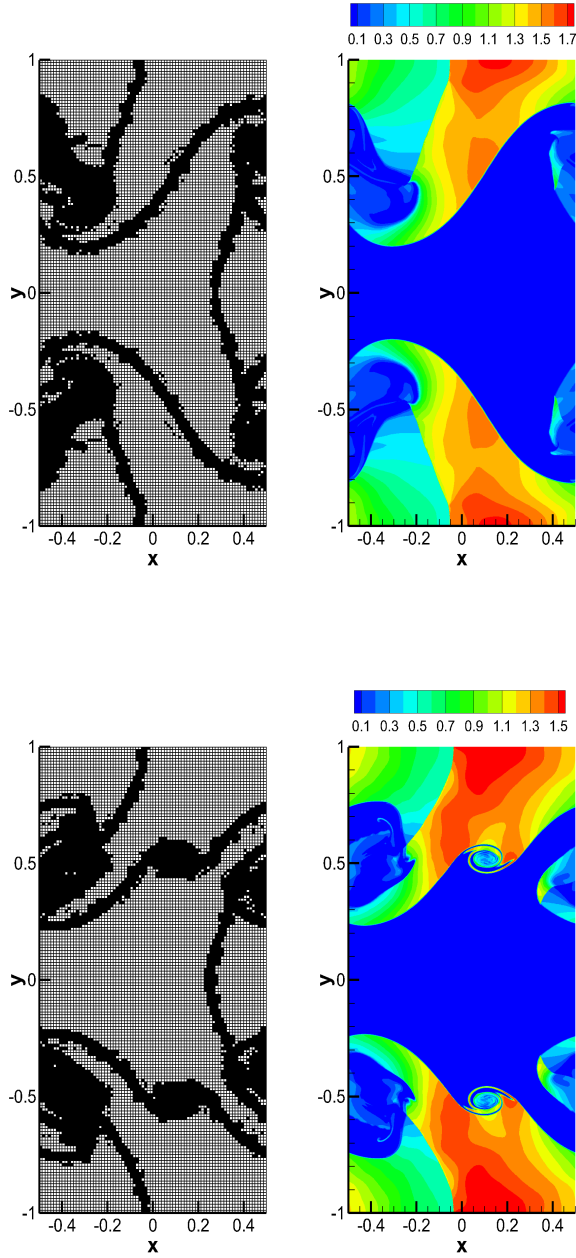


Figure 8: Two-dimensional Kelvin-Helmholtz instability at $t = 3.0$ with **refinement factor** $\tau = 4$. Left panels: the AMR grid. Right panels: the distribution of the rest-mass density. Top panels: results obtained with the HLL Riemann solver. Bottom panels: results obtained with the Osher Riemann solver. In both cases a third order ADER-WENO with CFL=0.8 has been adopted.

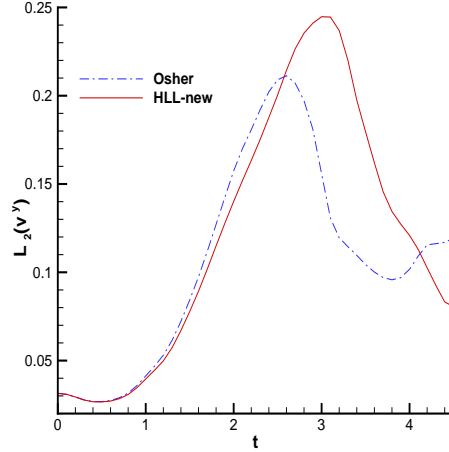


Figure 9: Time evolution of the L_2 norm of v^y showing the transition from the linear to the non-linear phase of the KH instability, occurring for $t \in [2, 3]$. The comparison between HLL and Osher is also shown.

bottom panels in each figure). Second, although the Osher-type Riemann solver is clearly able to capture the formation of tiny structures, by increasing the resolution the number of produced vortices decreases. This is evident after comparing the bottom panels of Fig. 7 and Fig. 8 which, at the reported time $t = 3$, have 269,858 and 627,024 cell elements, respectively. This result suggests that these secondary instabilities do not have a clear physical origin, and confirms what already found by Radice and Rezzolla (2012).

The growth scale of the instability is instead shown in Fig. 9, where the L_2 norm of the transverse velocity v^y is plotted as a function of time. The transition from the linear to the non-linear regime occurs for $t \in [2, 3]$ and it is slightly delayed when the diffusive HLL solver is used.

4.6. Three-dimensional spherical explosion

In order to validate the numerical scheme also in three spatial dimensions, we solve the special relativistic explosion problem on the computational domain $\Omega = [-1; 1]^3$, with initial conditions given by

$$(\rho, v, p) = \begin{cases} (1.0, 0, 1) & \text{for } r \leq R, \\ (0.125, 0, 0.1) & \text{for } r > R, \end{cases} \quad (43)$$

where the radial coordinate $r = \sqrt{x^2 + y^2 + z^2}$, while $R = 0.4$ denotes the radius of the initial discontinuity. In practice, the initial flow variables take the same constant values of the classical Sod's problem (Sod, 1978). The adiabatic index of the ideal-gas equation of state has been set to $\gamma = 4/3$. Due to the symmetry of the problem, the solution can be compared with an equivalent one dimensional problem in the radial direction r , which we have solved using the ECHO code by Del Zanna et al. (2007) with a high resolution uniform grid composed of 3000 cells. The

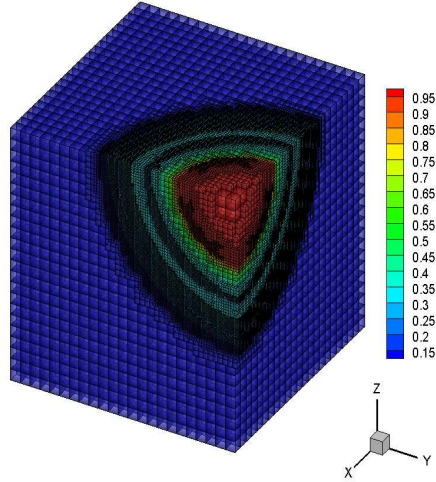


Figure 10: AMR grid structure at time $t = 0.25$ in the spherical explosion problem. The color contour of the rest-mass density is also shown.

initial grid at level zero of this three-dimensional problem uses $48 \times 48 \times 48$ cells, while during the evolution we have chosen $\tau = 2$ and $\ell_{\max} = 3$. We have performed a calculation at third order accuracy with the Osher-type Riemann solver and reconstruction in characteristic variables. The AMR grid at the final time $t = 0.25$ is shown in Fig. 10 and is formed by 7,044,376 elements. We stress that the a totally refined uniform grid corresponding to this configuration would be composed by 56,623,104 elements. One dimensional profiles of the most relevant quantities along the x axis are reported in the four panels of Fig. 11. A very good agreement with the one-dimensional reference solution is obtained.

5. Conclusions

Extending our recent work about classical gas dynamics (Dumbser et al., 2013), we have presented the first implementation of ADER methods in combination with Adaptive Mesh Refinement for the solution of the special relativistic hydrodynamics equations. The key idea of the ADER strategy, in the modern version proposed by Dumbser et al. (2008b), is to build high order accurate one-step finite volume schemes which are based on a high order nonlinear WENO reconstruction operator and an element-local weak formulation of the governing partial differential equations in space-time. This property becomes particularly advantageous in the presence of AMR, since, by avoiding the sub-steps typical of Runge-Kutta schemes, it substantially reduces the amount of necessary MPI communications and makes the implementation of time-accurate local time stepping (LTS) very natural and simple. Our AMR implementation follows a 'cell-by-cell' refinement criterion through a tree-data structure, similarly to Khokhlov et al. (1997).

We have verified the ability of our new scheme in coping with complex physical conditions, by considering a wide set of relativistic hydrodynamic tests, both for one and for multi-dimensional problems. Our ADER-WENO AMR scheme represents the first step of a plan to

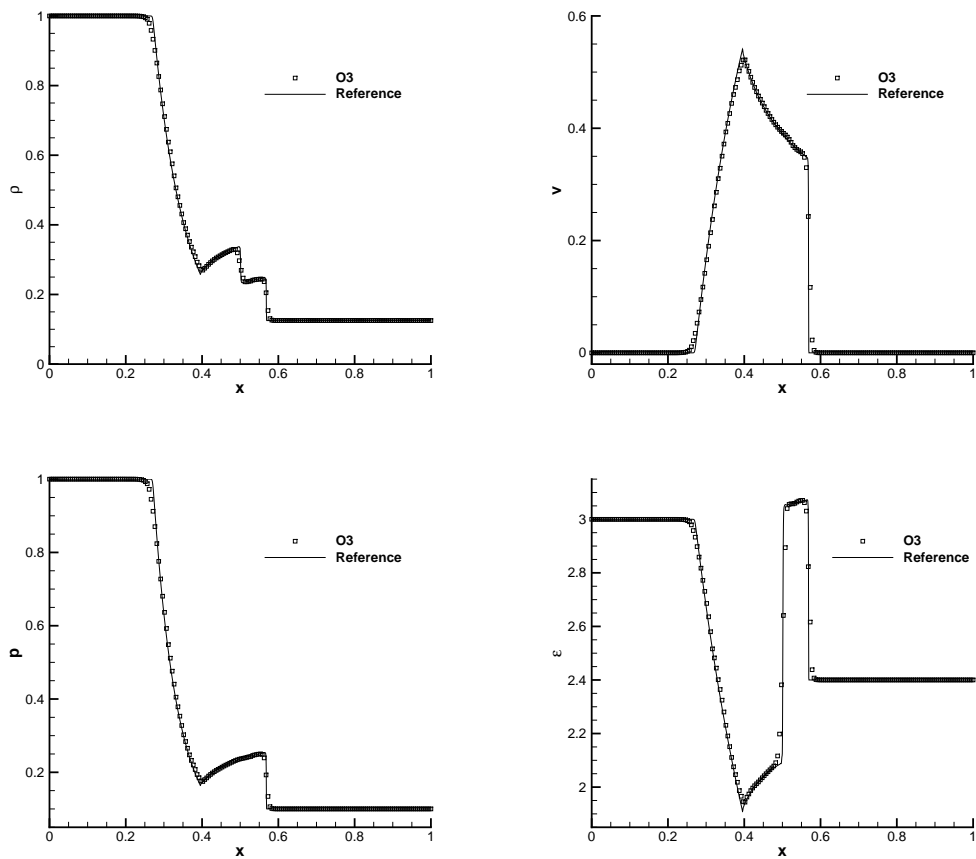


Figure 11: Explosion test in three space dimensions. From top left to bottom right: comparison of the 1D reference solution with the numerical solution obtained with a third order ADER-WENO scheme on an AMR mesh at time $t = 0.25$. One-dimensional cuts along the x -axis are shown for density, velocity, pressure and specific internal energy. Note that the plotted numerical data are the result of an interpolation, and are uniformly distributed.

incorporate more physical effects (magnetic fields, radiation hydrodynamics etc.) into a versatile tool suitable for studying high energy relativistic processes in astrophysics with high order of accuracy in both space and time.

High order methods often become the only choice for problems characterized by a wide range of length-scales, and in particular when fluid instabilities are triggered. One of such cases is represented by the Richtmyer-Meshkov (RM) instability, which arises when a shock wave crosses the interface between two fluids having different densities. The RM instability is thought to play a significant role in several high energy physical systems, including inertial confinement fusion (ICF) and core-collapse supernovae explosions. Broadly speaking, it typically produces a pronounced mixing of the involved fluids. Relativistic effects on the RM instability have been considered only recently (Inoue, 2012; Matsumoto and Masada, 2013; Mohseni et al., 2013), showing, somewhat counter-intuitively, that the growth rate of the instability decreases as the Lorentz factor increases. In the near future we plan to shed light on these aspects by means of high order numerical simulations combined with space-time adaptive mesh refinement.

Acknowledgments

The research conducted here has been financed in parts by the European Research Council under the European Union's Seventh Framework Programme (FP7/2007-2013) in the frame of the research project *STiMulUs*, ERC Grant agreement no. 278267.

The numerical simulations presented in this paper were performed on the FERMI Supercomputer at CINECA (Italy), within the IsB05-STiMulUs project, and on the SuperMuc at Leibniz-Rechenzentrum (Germany), within the PRACE 6-th CALL (Project ID 2012071312).

References

- M.A. Aloy, J.M. Ibáñez, J.M. Martí, E. Müller, *Astrophys. J. Suppl.* 122 (1999) 151–166.
- M.A. Aloy, L. Rezzolla, *Astrophys. J.* 640 (2006) L115–L118.
- M. Anderson, E. Hirschmann, S.L. Liebling, D. Neilsen, *Classical Quantum Gravity* 23 (2006) 6503–6524.
- A.M. Anile, *Relativistic Fluids and Magneto-fluids*, Cambridge University Press, 1990.
- A.M. Anile, J.C. Miller, S. Motta, *Physics of Fluids* 26 (1983) 1450–1460.
- A. Baeza, A. Martínez-Gavara, P. Mulet, *Applied Numerical Mathematics* 62 (2012) 278–296.
- A. Baeza, P. Mulet, *International Journal for Numerical Methods in Fluids* 52 (2006) 455–471.
- L. Baiotti, *Numerical relativity simulations of non-vacuum spacetimes in three dimensions*, Ph.D. thesis, SISSA, International School for advanced studies, 2004.
- K. Beckwith, J.M. Stone, *The Astrophysical Journal Supplement Series* 193 (2011) 6.
- M.J. Berger, *SIAM Journal of Scientific and Statistical Computing* 7 (1986) 904–916.
- M.J. Berger, P. Colella, *J. Comput. Phys.* 82 (1989) 64–84.
- M.J. Berger, J. Olinger, *J. Comput. Phys.* 53 (1984) 484–512.
- N. Bucciantini, L. Del Zanna, *Astron. Astrophys.* 528 (2011) A101.
- M.W. Choptuik, in: C. Evans, L. Finn, D. Hobill (Eds.), *Frontiers in Numerical Relativity*, Cambridge University Press, Cambridge, England, 1989, pp. 206–221.
- S. Clain, S. Diot, R. Loubère, *Journal of Computational Physics* 230 (2011) 4028–4050.
- F. De Colle, J. Granot, D. López-Cámara, E. Ramirez-Ruiz, *Astrophys. J.* 746 (2012) 122.
- L. Del Zanna, N. Bucciantini, *Astron. Astrophys.* 390 (2002) 1177–1186.
- L. Del Zanna, O. Zanotti, N. Bucciantini, P. Londrillo, *Astron. Astrophys.* 473 (2007) 11–30.
- A. Dolezal, *Journal of Computational Physics* 120 (1995) 266–277.
- O. Dönmez, *Astrophys. Spac. Sci.* 293 (2004) 323–354.
- M. Dumbser, D.S. Balsara, E.F. Toro, C.D. Munz, *Journal of Computational Physics* 227 (2008a) 8209–8253.
- M. Dumbser, C. Enaux, E.F. Toro, *Journal of Computational Physics* 227 (2008b) 3971–4001.
- M. Dumbser, M. Kaeser, V.A. Titarev, E.F. Toro, *Journal of Computational Physics* 226 (2007) 204–243.
- M. Dumbser, M. Kser, E.F. Toro, *Geophysical Journal International* 171 (2007) 695–717.

M. Dumbser, E. Toro, *Communications in Computational Physics* 10 (2011) 635–671.

M. Dumbser, O. Zanotti, *Journal of Computational Physics* 228 (2009) 6991–7006.

M. Dumbser, O. Zanotti, A. Hidalgo, D.S. Balsara, *Journal of Computational Physics* 248 (2013) 257–286.

W.E. East, F. Pretorius, B.C. Stephens, *Phys. Rev. D* 85 (2012) 124010.

Z.B. Etienne, Y.T. Liu, S.L. Shapiro, *Phys. Rev. D* 82 (2010) 084031.

E. Evans, S. Iyer, E. Schnetter, W.M. Suen, J. Tao, R. Wolfmeyer, H.M. Zhang, *Phys. Rev. D* 71 (2005) 081301(R).

J.A. Font, *Living Rev. Relativ.* 6 (2008) 4; <http://www.livingreviews.org/lrr-2008-7>.

G. Gassner, F. Lörcher, C.D. Munz, *Journal of Scientific Computing* 34 (2008) 260–286.

A. Harten, P.D. Lax, B. van Leer, *SIAM Rev.* 25 (1983) 35.

T. Inoue, *Astrop. J.* 760 (2012) 43.

A.M. Khokhlov, E.S. Oran, J.C. Wheeler, *Astrophys. J.* 478 (1997) 678.

L. Lehner, C. Palenzuela, S.L. Liebling, C. Thompson, C. Hanna, *Phys. Rev. D* 86 (2012) 104035.

S.L. Liebling, L. Lehner, D. Neilsen, C. Palenzuela, *Phys. Rev. D* 81 (2010) 124023.

R. Löhner, *Computer Methods in Applied Mechanics and Engineering* 61 (1987) 323–338.

F. Lörcher, G. Gassner, C.D. Munz, *Journal of Scientific Computing* 32 (2007) 175–199.

A. Lucas-Serrano, J.A. Font, J.M. Ibanez, J.M. Martí, *Astron. Astrophys.* 428 (2004) 703–715.

P. MacNeice, K.M. Olson, C. Mobarry, R. de Fainchtein, C. Packer, *Computer Physics Communications* 126 (2000) 330–354.

J.M. Martí, J.M. Ibáñez, J.A. Miralles, *Phys. Rev. D* 43 (1991) 3794.

J.M. Martí, E. Müller, *J. Fluid Mech.* 258 (1994) 317–333.

J.M. Martí, E. Müller, *Living Rev. Relativ.* 6 (2003) 7; <http://www.livingreviews.org/lrr-2003-7>.

J. Matsumoto, Y. Masada, *Astrop. J. Lett.* 772 (2013) L1.

A. Mignone, G. Bodo, *Mon. Not. R. Astron. Soc.* 364 (2005) 126–136.

A. Mignone, M. Ugliano, G. Bodo, *Monthly Notices of the Royal Astronomical Society* 393 (2009) 1141–1156.

A. Mignone, C. Zanni, P. Tzeferacos, B. van Straalen, P. Colella, G. Bodo, *Astrophys. J. Suppl. Ser.* 198 (2012) 7.

F. Mohseni, M. Mendoza, S. Succi, H.J. Herrmann, *ArXiv e-prints* (2013).

D. Radice, L. Rezzolla, *Phys. Rev. D* 84 (2011) 024010.

D. Radice, L. Rezzolla, *Astron. Astrophys.* 547 (2012) A26.

L. Rezzolla, O. Zanotti, *Journ. of Fluid Mech.* 449 (2001) 395.

L. Rezzolla, O. Zanotti, *Phys. Rev. Lett.* 89 (2002) 114501.

L. Rezzolla, O. Zanotti, *Relativistic Hydrodynamics*, Oxford University Press, Oxford UK, 2013.

L. Rezzolla, O. Zanotti, J.A. Pons, *Journ. of Fluid Mech.* 479 (2003) 199.

G.A. Sod, *Journal of Computational Physics* 27 (1978) 1–31.

P. Solin, *Partial Differential Equations And the Finite Element Method*, Pure and Applied Mathematics, Wiley-Interscience, 2006.

J. Tao, W.M. Suen, R. Wolfmeyer, H.M. Zhang, in: *APS April Meeting Abstracts*, p. K1012.

A. Taube, M. Dumbser, C.D. Munz, R. Schneider, *International Journal of Numerical Modelling: Electronic Networks, Devices and Fields* 22 (2009) 77–103. Cited By (since 1996):9.

A. Tchekhovskoy, J.C. McKinney, R. Narayan, *Mon. Not. R. Astron. Soc.* 379 (2007) 469–497.

E.F. Toro, V.A. Titarev, *Proceedings of the Royal Society of London. Series A: Mathematical, Physical and Engineering Sciences* 458 (2002) 271–281.

E.F. Toro, V.A. Titarev, *Journal of Computational Physics* 202 (2005) 196–215.

B. van der Holst, R. Keppens, Z. Meliani, *Computer Physics Communications* 179 (2008) 617–627.

K.H.A. Winkler, M.L. Norman, D. Mihalas, *Journal of Quantitative Spectroscopy and Radiative Transfer* 31 (1984) 473–478.

O. Zanotti, M. Dumbser, *Mon. Not. R. Astron. Soc.* 418 (2011) 1004–1011.

W. Zhang, A. MacFadyen, *The Astrophysical Journal Supplement Series* 164 (2006) 255.